Fibers and Polymers 2017, Vol.18, No.2, 212-220
DOI 10.1007/s12221-017-6772-0

ISSN 1229-9197 (print version)
ISSN 1875-0052 (electronic version)

Electrospun SiO_2/PMIA Nanofiber Membranes with Higher Ionic Conductivity for High Temperature Resistance Lithium-ion Batteries

Yafang Li[1], Xiaomin Ma[1], Nanping Deng[1], Weimin Kang[1,2]*, Huihui Zhao[1], Zongjie Li[1], and Bowen Cheng[2]*

[1]*School of Textiles, Tianjin Polytechnic University, Tianjin 300387, China*
[2]*State Key Laboratory of Separation Membranes and Membrane Processes, Tianjin Polytechnic University, Tianjin 300387, China*

(Received July 25, 2016; Revised October 27, 2016; Accepted October 30, 2016)

Abstract: The nanofiber membrane prepared by electrospinning has been widely applied in lithium-ion batteries. A powerful strategy for designing, fabricating and evaluating Poly-*m*-phenylene isophthalamide (PMIA) nanofiber membrane with SiO_2 nanoparticles was developed by electrospinning in this paper. The morphology, crystallinity, thermal shrinkage, porosity and electrolyte uptake, and electrochemical performance of the SiO_2/PMIA nanofiber membranes were investigated. It was demonstrated that the nanofiber membrane with 6 wt% SiO_2 possessed notable properties, such as better thermal stability, higher porosity and electrolyte uptake, resulting in higher ionic conductivity (3.23×10^{-3} $S\cdot cm^{-1}$) when compared with pure PMIA nanofiber membrane. Significantly, the SiO_2/PMIA nanofiber membrane based Li/$LiCoO_2$ cell exhibited more excellent cycling stability with capacity retention of 95 % after 50 cycles. The results indicated that the SiO_2-doped PMIA nanofiber membranes had a potential application as separator in high temperature resistance lithium-ion batteries.

Keywords: Lithium-ion battery, Electrospinning, PMIA nanofiber membrane, SiO_2, Electrochemical performance

Introduction

Lithium-ion batteries as an efficient energy storage system for a wide variety of new energy vehicles have attracted more and more attentions because of high energy density, big power density, long cycle life and low memory effect [1-4]. In a lithium-ion battery, the separator plays an essential role in preventing the physical electronic contact between electrodes and serves as a liquid electrolyte reservoir to transport ions [5-7]. Due to good chemical stability, suitable thickness and enough mechanical strength, the commercially polyolefin (PE) microporous membranes have been widely used as the lithium-ion battery separators. However, their intrinsic limitations are not conducive to the passing of lithium ions because of low porosity and electrolyte wettability. Moreover, the poor thermal shrinkage leads to the short circuit easily, which limits its application prospects in the Power Battery [8-11].

In order to make the lithium-ion battery separators have a better development, a lot of methods have been studied, including γ-ray irradiation method [12], solvent casting technique [13], thermally induced phase separation technique [14], phase inversion method [15], and electrospinning technique [16-18]. Among those, electrospinning is a promising method and the nanofiber membranes prepared by electrospinning have a great potential in separator materials for lithium-ion batteries due to the high electrolyte uptake and ionic conductivity. Meanwhile, the nanofiber membranes can make electrons and ions transport easier between electrodes, thus not only significantly improve the cycle performance of batteries, but also can prolong the service life of batteries [19-22]. Various electrospun membranes from different polymer materials have been attempted as separators of lithium-ion batteries, including polyacrylonitrile (PAN) [23], Poly(vinylidene fluoride) (PVdF) [24,25], poly(vinylidene fluoride co-hexafluoropropylene) (PVdF-HFP) [26], and polyethylene terephthalate (PET) [27] etc. Thanks to the more sophisticated electrospinning technology, membranes with heat-resistant engineering polymers, such as poly(phthalazinone ether sulfone ketone) (PPESK) [28], polyimide (PI) [29,30] etc., as the matrix, have attracted lots of attentions in recent years.

As we all known, the aramid fiber is a kind of high-performance fiber with superior strength and modulus, low density and good wear resistance [31]. Poly-*m*-phenylene isophthalamide (PMIA) with monomers of m-phenylenediamine and isophthalic acid is the zigzag macromolecule with neatly arrangement. It is widely applied to the high temperature filter materials, special protective clothing, electrical insulating materials, honeycomb structure wainscoting materials, etc., due to its outstanding performances, such as excellent thermal resistivity (T_g=270 °C), self-extinguishing characteristics, chemical resistance, mechanical properties and electrical insulation ability. Meanwhile, it will not be decomposed and carbonized below 350 °C [32,33]. In recent years, PMIA fiber membrane applied into lithium-ion batteries has been researched by many scholars. Zhang *et al.* [34] explored the aramid as lithium-ion battery separator via a papermaking process. It demonstrated that the membrane as battery separators had a better performance than PP separators on electrolyte wettability, thermal resistance, cycle performance and so on. Zhai *et al.* [32] fabricated sandwich-structured PVdF/PMIA/PVdF nanofibrous battery separators with

*Corresponding author: kweimin@126.com
*Corresponding author: bowen15@tjpu.edu.cn

possessing shutdown function via a sequential electrospinning technique. Meanwhile, the composite membranes increased tensile strength (13.96 MPa). Subsequently, they also prepared the nanonet-structured PMIA-PU nanofibrous membranes with enhanced thermostability, good wettability and high ionic conductivity up to 1.38 $S \cdot cm^{-1}$ [35]. Although the practicability of PMIA polymer membranes as lithium-ion battery separators was confirmed, the optimal electrolyte uptake and ionic conductivity had not been achieved.

The implantation of inorganic components, such as TiO_2, SnO_2, MgO, Al_2O_3, and SiO_2, has been proved to enhance thermal stability, electrolyte uptake and ionic conductivity of nanofiber membranes by increasing amorphous region [36-39]. Juang *et al.* [36] reported TiO_2-coated PP/PE/PP composite separators, which enhanced thermal stability and featured a highly porous structure, allowing favorable liquid wettability and high mass uptake of electrolyte. Jeon *et al.* [37] coated the electrospun meta-aramid nanofiber membrane with Al_2O_3, and the thermal stability of the modified gel polymer electrolyte was proved to be greatly elevated. Yanilmaz *et al.* [38] prepared a SiO_2/PVDF hybrid membrane with higher lithium ion transference and ion conductivity (2.6×10^{-3} $S \cdot cm^{-1}$) by dispersing 24 % SiO_2 nanoparticles onto PVDF nanofiber surfaces.

In this work, a valid method was used to prepare nanofiber separators by combining the advantages of electrospinning membrane with the modification of SiO_2 nanoparticles. The physical properties of electrospinning fiber membranes and the electrochemical properties of fibrous polymer electrolytes using for lithium-ion batteries were investigated. The results demonstrated that the fabricated membrane possessed some excellent properties, such as good thermal stability, high porosity and electrolyte uptake, and great electrochemical performance for lithium-ion batteries. Thus, the high temperature resistance lithium-ion battery separators would have a better developmental prospect for the hybrid vehicles.

Experimental

Materials

Poly-*m*-phenylene isophthalamide (PMIA, industrial grade) was purchased from Yantai Spandex Co. Ltd., China. N,N-dimethyl acetamide (DMA_C) and SiO_2 nanoparticles (diameter of particles, ≤30 nm) were purchased from Tianjin Kermel Chemical Reagent Co. Ltd., China. The selected liquid electrolyte was provided by Tianjin Jinniu Power Materials Co. Ltd., China, which was prepared by dissolving 1 mol/*l* $LiPF_6$ in ethylene carbonate (EC)/diethyl carbonate (DMC) (1:1 by volume) solution. The chemical reagents were all purchased commercially and used without further purification.

Fabrication of SiO_2/PMIA Nanofiber Membrane

The blend membranes were prepared by the electrospun technique. SiO_2/DMAc dispersed solution was prepared by adding SiO_2 nanoparticles into DMAc with slight dispersant and then ultrasonically agitated for 15 minutes after vigorously stirring for 10 minutes. The obtained SiO_2/DMAc dispersed solution was added to PMIA/DMAc spinning dope with a certain concentration. Then the SiO_2/PMIA nanofiber membranes with 0 wt%, 2 wt%, 4 wt%, 6 wt%, and 8 wt% SiO_2 (mass ratio based on the weight of PMIA) was prepared, respectively. The solution was taken in the syringe and delivered with a flow rate of 0.2 m*l*/h. A potential difference of 25 kV was kept between the nozzle of the syringe and the collector (aluminum drum) at room temperature. A metering pump was used to control the flow rate. A distance of 16 cm was kept between the syringe tip and the collector. Dry fibers accumulated on the collector (drum) were collected as fibrous membranes. Electrostatic spinning equipment was made by our research group.

Electrode Preparation and Cell Assembly

CR2032 coin-type cells were assembled in an argon-filled glove box by sandwiching a separator between a lithium metal anode and a lithium cobalt oxide (85 wt% $LiCoO_2$, 10 wt% carbon black and 5 wt% binder (polytetrafluoroethylene, PTFE) on aluminum foil) and activated by the electrolyte (1 mol/*l* $LiPF_6$ in EC/DMC (1:1 by volume) solution).

Physical and Electrochemical Characterizations

Morphology

The surface morphology of relevant membranes was examined by using high resolution field-emission scanning electron microscope (FE-SEM, S-4800, Hitachi Ltd., Japan). The internal structure of fibers was examined by using transmission electron microscope (TEM, H-7650, Hitachi Ltd., Japan).

XRD

X-ray diffraction (XRD) patterns were recorded using D/MAX-2500 X-ray diffractometer (Rigaku Corporation) with Cu Kα radiation in the 2θ range between 0 and 50 °.

Electrolyte Uptake and Porosity

The electrolyte uptake was obtained by the equation (1).

$$\text{Electrolyte uptake} = \frac{M_w - M_d}{M_d} \times 100\% \quad (1)$$

where M_d and M_w are the mass of membranes before and after immersion in electrolyte ($LiPF_6$ in EC/DMC (1:1 by volume)) for 24 h, respectively.

Porosity of membranes was measured by immersing membranes in n-butanol (Yingda Chemical Co., Ltd.) for 2 h. The porosity (%) of the membranes was calculated by the equation (2).

$$\text{Porosity} = \frac{M_a - M_b}{\rho_b V_m M_b} \times 100\% \quad (2)$$

where M_b and M_a are the mass of membrane before and after immersion respectively, ρ_b is the density of n-butanol and V_m

is the volume of the membrane before immersion.

Mechanical Properties

The mechanical property of membranes was measured using YG005 Electronic Single Fiber Strength Tester (Fangyan Instrument Co., Ltd., China) at the extension rate of 10 mm·min^{-1}. The dimensions of the examined samples were 40 mm×5 mm (length and width). The unit X (cN) of the tested values can be transformed to Y (MPa) by equation (3).

$$Y\,(\mathrm{MPa}) = \frac{X\,(cN)}{A\,(\mathrm{cm}) \cdot B\,(\mu\mathrm{m})} \tag{3}$$

where A is the width and B is the thickness of membranes. The thickness of membrane was measured with a 0-10-3Q thickness gauge (Shanghai chuanlu measuring tool Co., Ltd.).

Thermal Stability

The thermal performance were characterized by TGA (thermogravimetric analysis) from 25 °C to 900 °C under nitrogen at a heating rate of 10 °C·min^{-1}. Furthermore, the heat shrinkage property was tested by comparing the dimensional changes of the membranes after thermal treatment at various temperatures for 30 min.

Electrochemical Properties

The ionic conductivity of relevant membranes was measured by AC impedance method using CHI660D electrochemical workstation. The electrolytes were placed between a pair of stainless-steel blocking electrodes and the frequency was the range of 10^{-2}-10^{6} Hz at room temperature with the amplitude of 1 mV. The ionic conductivity was obtained by equation (4).

$$K = \frac{d}{R \times S} \tag{4}$$

where d is the thickness of the GPE membranes (μm); R is the bulk resistance of the GPE (Ω); S is the contact area between GPE and SS (m^2). The thickness of the films can be measured by Absolute Digimatic Thickness Gauge (547-401, Mitutoyo) with the range of 0.001 mm.

Electrochemical stability was determined by linear sweep voltammetry method using CHI660D electrochemical analyzer at a scan rate of 5 mV·s^{-1} with voltage from 2.8-6.0 V. Cycling performance were performed between 2.8 V and 4.2 V at a current density of 0.1 C with a battery test system provided by Wuhan LISUN Co., Ltd., China.

Results and Discussion

Morphology

The SEM, TEM and diameter distribution images of PMIA nanofiber membranes with 0 wt%, 2 wt%, 4 wt%, 6 wt% and 8 wt% SiO_2 are shown in Figure 1. It was observed that the pure PMIA and composite membranes had a three-dimensional network structure interconnected with a large number of voids and cavities of different sizes. There was no bead formation under the suitable conditions of the electrospinning. The average fiber diameters tend to increase due to the increase of viscosity with the addition of SiO_2. The solution consisting of more SiO_2 must overcome higher liquid inside friction to flow. As can be seen clearly in SEM and TEM images, the tiny SiO_2 nanoparticles could adhere to the surface of fibers uniformly when the content of SiO_2

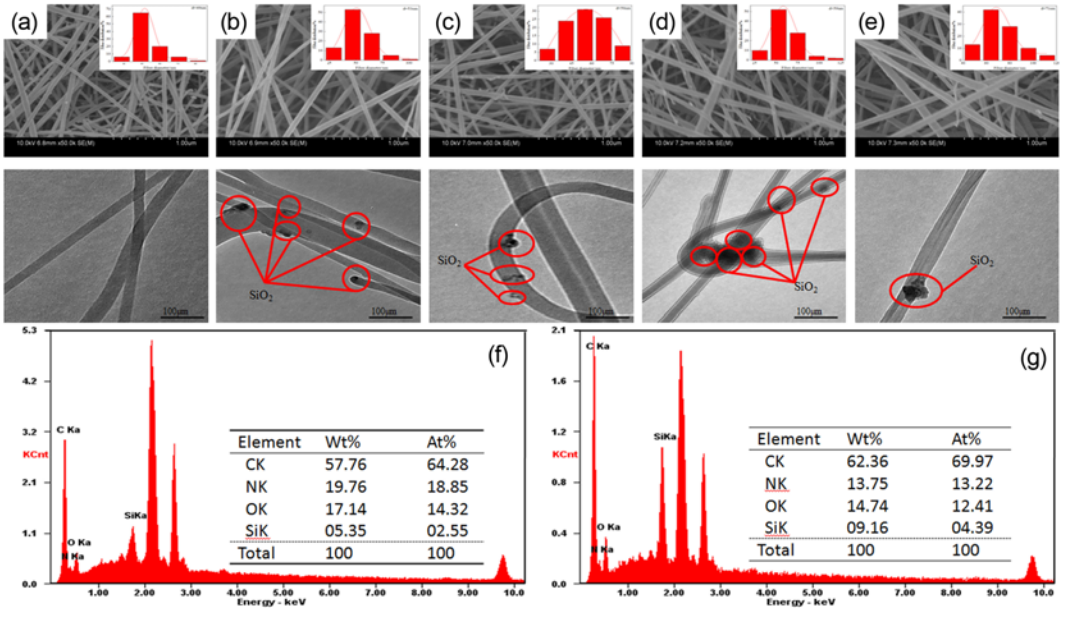

Figure 1. SEM, TEM, and diameter distribution images of PMIA nanofiber membranes with different SiO_2 contents ((a) 0 %, (b) 2 %, (c) 4 %, (d) 6 %, and (e) 8 %) and EDS spectra of PMIA nanofiber membranes with (f) 2 % and (g) 4 % SiO_2 contents.

was lower than 6 wt%. Meanwhile, the composite nanofibers had rougher surface obviously, thus could contribute to enhance the absorption of electrolyte [39-41]. However, SiO_2 nanoparticles on the fiber surface showed obvious agglomeration phenomenon and agglomerated particle diameters reach 100 nm under the condition of 8 wt% SiO_2.

The presence of SiO_2 nanoparticle within the fiber was investigated by energy dispersive spectroscopy (EDS). The EDS spectra of PMIA nanofiber membranes with 2 % and 4 % SiO_2 contents are shown in Figure 1(f) and (g), respectively. It was observed that the characteristic peak of Si element appeared at 1.8 KeV. Additionally, compared with 2 wt% SiO_2 doped membrane, the content of Si element obviously increased in 4 wt% SiO_2 doped membrane which was demonstrated by higher intensity in EDS spectrum and corresponding data. The result was in accordance with the constituent content of spinning solution.

XRD

XRD patterns of SiO_2/PMIA membranes with various SiO_2 contents are presented in Figure 2 (2θ=25 ° is marked by the black dashed line). It could be seen that pure PMIA nanofiber membrane and SiO_2-doped PMIA nanofiber membranes all had some prominent diffraction peak at 2θ=25 °. Moreover, the diffraction peak intensity broadened gradually with the increase of SiO_2 content, which showed a decrease in both crystalline size and the degree of crystallinity. This is attributed partly to Lewis acid-base interactions between the polymer matrix and the deposited SiO_2 and partly to more crosslinking sites for polymer chains [42]. Thus could greatly improve electrolyte uptake of membrane [43]. In addition, there was no new diffraction peak in XRD spectrum, which demonstrated that triclinic system of PMIA did not change with the addition of SiO_2 nanoparticles.

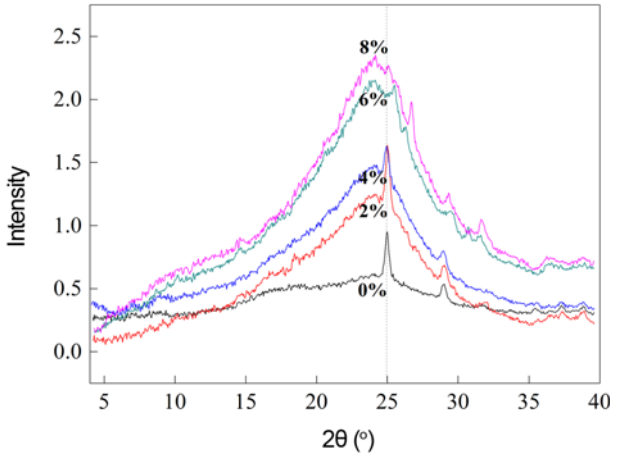

Figure 2. XRD patterns of PMIA nanofiber membranes with different SiO_2 contents.

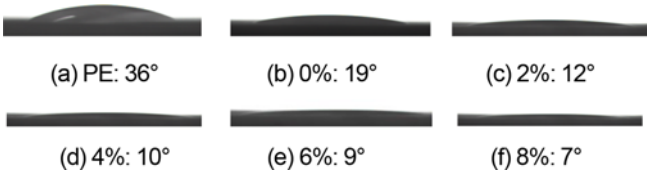

Figure 3. Contact angle of PE separator (a) and PMIA nanofiber membranes with different SiO_2 contents (b) 0 %, (c) 2 %, (d) 4 %, (e) 6 %, and (f) 8 %.

Wettability

The wettability is one of important factors for evaluating the performance of lithium ion battery separators, because the separator can absorb and hold amount of liquid electrolyte. The wettability of PE and PMIA nanofiber membranes with different SiO_2 contents were evaluated by the water contact angles. The results and the photos during actual test are illustrated in Figure 3. It could be obviously observed that the contact angle of PE membrane was 36 °, which was higher than pure PMIA nanofiber membrane (19 °). The contact angle of SiO_2/PMIA membranes dropped down gradually with the increase of SiO_2 content. This is because the higher inorganic nanoparticle specific surface area is beneficial to absorption of the electrolyte, which can lead to the decrease of contact angle [44].

Porosity and Electrolyte Uptake

The porosity and electrolyte uptake are important factors to determine the ionic conductivity and electrochemical properties of battery separators. The size of porosity directly affected the electrolyte uptake of separators to determine absorptive capacity and storage capacity of battery separators for electrolyte. Thus can directly affect the cycle life and high-rate charge-discharge ability of batteries. The porosity and electrolyte uptake of PMIA nanofiber membranes with different SiO_2 contents are shown in Figure 4 and Figure 5, respectively.

As shown in Figure 4, SiO_2/PMIA membranes had a higher porosity compared with pure PMIA membrane. At the same time, porosity was gradually increasing from 74 % to 92 % with the increasing of SiO_2 contents. Furthermore, in Figure 5, the electrolyte uptake of SiO_2/PMIA composite membranes had a significantly improvement when compared with pure PMIA membrane. The excellent porosity and electrolyte uptake of SiO_2/PMIA membranes is mainly attributed to the following three reasons. Firstly, the addition of SiO_2 can make the fiber surface rougher to improve the porosity. High porosity is favorable to reducing the internal resistant and improving the ionic conductivity. Secondly, the higher SiO_2 specific surface area is beneficial to absorption of the electrolyte. Finally, the fibers prepared by the electrostatic spinning are porous network and the average diameters of SiO_2/PMIA nanofibers become higher with the rise of SiO_2 component, which builds more space in the fiber structure.

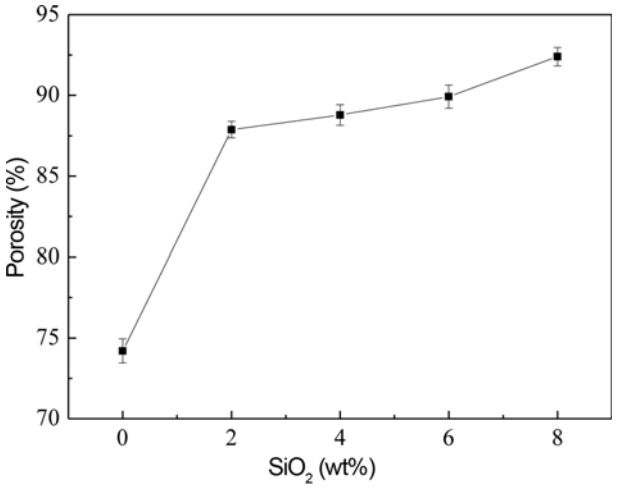

Figure 4. Porosity of nanofiber membranes with different SiO_2 contents.

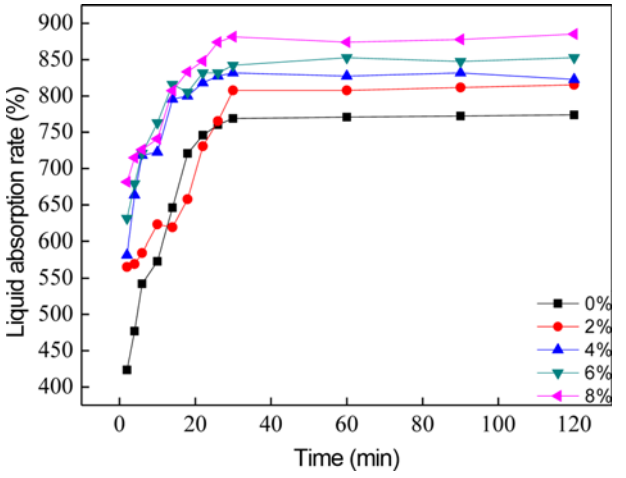

Figure 5. Electrolyte uptake of nanofiber membranes with different SiO_2 contents; 0 %, 2 %, 4 %, 6 %, and 8 %.

Mechanical Properties

High mechanical strength is needed in separator to improve the safety performance of batteries. As can be seen in Figure 6, the stress-strain curves of membranes showed a linear elastic deformation. The tensile strength and breaking elongation rate of pure nanofiber membrane were 8.75 MPa and 19.40 %, respectively. However, after the addition of SiO_2 nanoparticles, the breaking strength of membranes was greatly improved. This is due to the fact that molecular chain form a three-dimensional network structure by attractive interaction of van der Waals force, electrostatic attraction, polar groups of SiO_2 surface and atoms of PMIA molecular chain. When the membranes subject to the external force, the stress could be dispersed to other molecular chains by network structure junction. Thus even if one molecular chain breaks, the others can still work. As shown in Figure 6, when

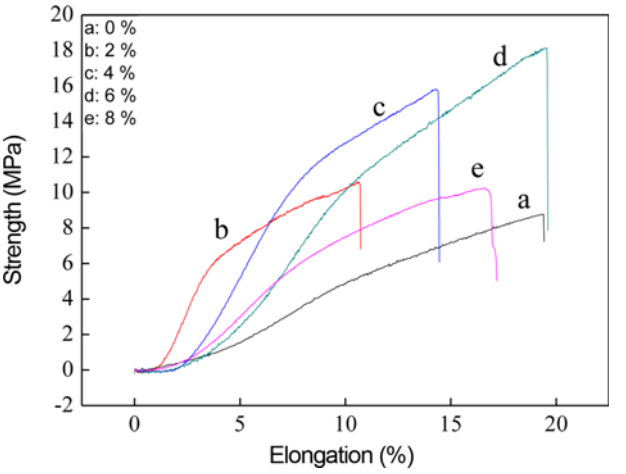

Figure 6. Stress-strain curves of nanofiber members with different SiO_2 contents; (a) 0 %, (b) 2 %, (c) 4 %, (d) 6 %, and (e) 8 %.

SiO_2 content was 6 wt%, the breaking strength and breaking elongation rate reached a maximum, which were 18.14 MPa and 19.50 %, respectively; while SiO_2 content was 8 wt%, both breaking strength and breaking elongation rate began to decrease. This is because the overweight of SiO_2, nanoparticles produce agglomeration to reduce mechanical strength of fiber membranes.

Thermal Stability

The TG (a) and DTG (b) of SiO_2/PMIA separators with different SiO_2 contents are shown in Figure 7. In Figure 7(a), a fall point happened at about 250 °C, which was mainly attributed to the volatilization of the added dispersant for SiO_2 and small molecule additive from PMIA stock solution; another fall point began at about 400 °C, which was considered to the initial decomposition temperature of the PMIA macromolecular chains. As can be known from Figure 7(b), it can be obviously observed that the decomposition peak temperature of nanofiber membranes rise after the addition of SiO_2. This may be because SiO_2 nanoparticles suppress the movement of PMIA molecules, so that PMIA need more energy to decompose. Therefore, the higher decomposition temperature can be obtained. The curves did not change obviously any more with the temperature rising continually. This states that organic phase PMIA and solvent in the fibers had been decomposed completely. At this time, there was only pure inorganic phase in the fiber membranes, and the samples had no mass loss. All of those showed that SiO_2/PMIA had an excellent thermal stability.

Thermal shrinkage of the separators is another important property related to both battery performance and safety characteristic. A superior thermal resistance can prevent internal electrical short circuit effectively and endow a better safety characteristic at elevated temperature when the batteries are subjected to high charge-discharged rates [45]. Figure 8

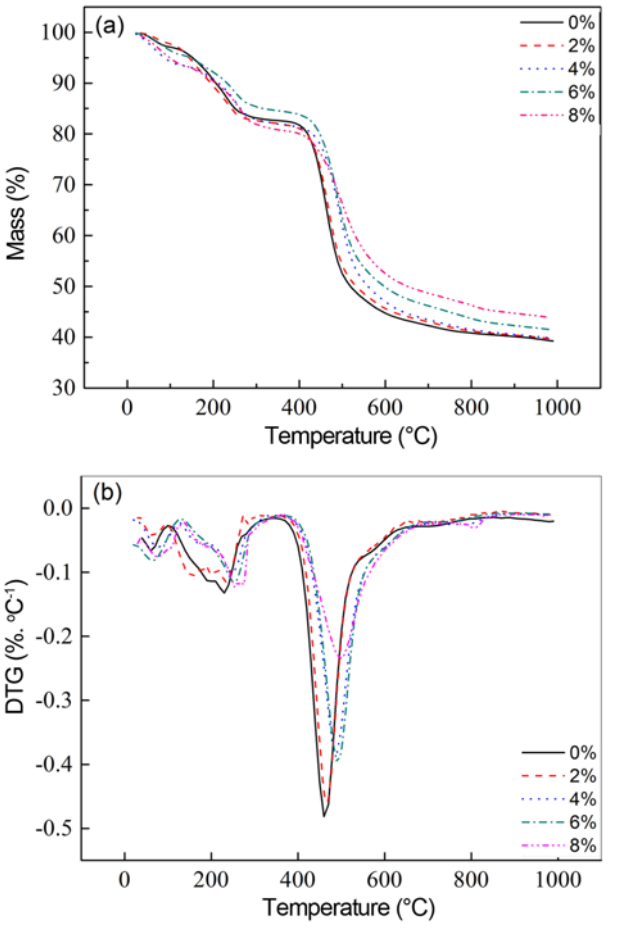

Figure 7. TG (a) and DTG (b) curves of SiO$_2$/PMIA separators with different SiO$_2$ contents; 0 %, 2 %, 4 %, 6 %, and 8 %.

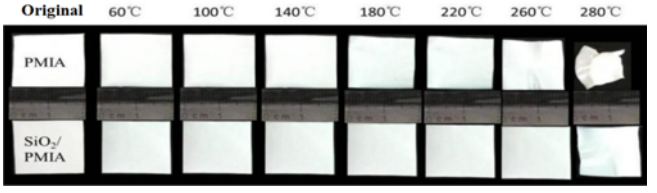

Figure 8. The photographs of pure PMIA and SiO$_2$/PMIA membranes after thermal treatment at different temperatures.

shows the heat shrinkage of pure PMIA membrane and SiO$_2$/PMIA membrane with 6 wt% SiO$_2$ content at free relaxation condition after thermal treatment at different temperatures. As can be seen that the area of both membranes had no shrinkage at 220 °C (microporous PP membrane was shrank at 150 °C [38]). When after being treated at 260 °C, the pure PMIA membrane had a slight deformation. While at 280 °C, SiO$_2$/PMIA membrane began to shrink. Therefore, the composite membrane exhibited a better dimensional stability compared to pure PMIA membrane.

Electrochemical Properties

Ionic Conductivities

The ionic conductivities obtained from the *z′* axis of high-frequency intercept of Nyquist plots with a cell (SS| separator | SS) are showed in Figure 9 and Figure 10. It was observed that the ionic conductivities of PMIA composite separators with different SiO$_2$ contents (2 wt%, 4 wt%, 6 wt%, 8 wt%) were 1.04×10^{-3} S·cm^{-1}, 2.25×10^{-3} S·cm^{-1}, 3.23×10^{-3} S·cm^{-1} and 1.75×10^{-3} S·cm^{-1}, respectively, which were much superior to PE separator (0.2×10^{-3} S·cm^{-1}) and pure PMIA separator (0.61×10^{-3} S·cm^{-1}). The results showed that the good pore interconnectivity and high porosity could improve the ionic conductivity of electrospinning SiO$_2$/PMIA composite membrane. Furthermore, the most important reason for the enhancement of conductivities is the association between the filler particle and the polymer chains and the

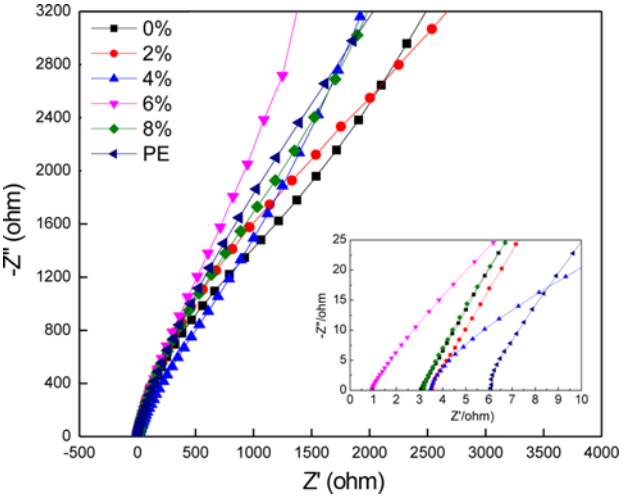

Figure 9. AC impedance spectra of liquid electrolyte-soaked SiO$_2$/PMIA separators with different SiO$_2$ contents; 0 %, 2 %, 4 %, 6 %, and 8 %.

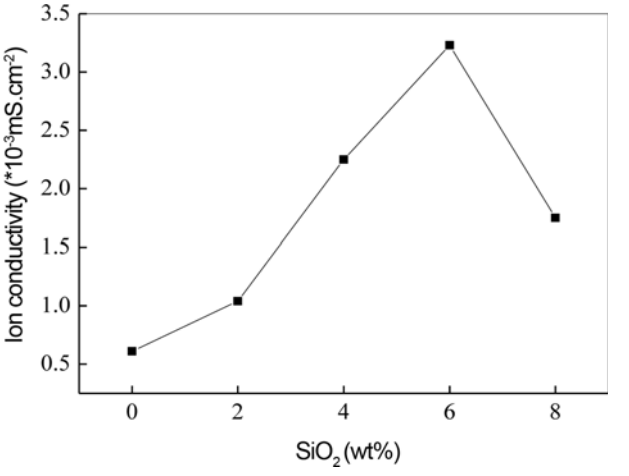

Figure 10. Ionic conductivity of SiO$_2$/PMIA separators with different SiO$_2$ contents and PE separator.

Lewis acid-base interactions between the SiO_2 particles and the electrolyte polar groups. Meanwhile, the ionic conductivity reached the maximum with the addition of 6 wt% SiO_2, which could greatly improve the charge-discharge capacity and was beneficial to quick charge-discharge ability on lithium-ion batteries. However, it began to decrease with the addition of 8 wt% SiO_2. This is mainly attributed to the specific interactions among inorganic particles, PMIA groups and lithium salt after the additive of amounts of inorganic particles. It can induce polymer chain of the particle surface structure change thereby affect ion agglomeration of organic-inorganic composite polymer electrolyte amorphous area. Meanwhile, it improves the agglomeration of PMIA molecular chain and accelerates the recrystallization rate [46,47].

Electrochemical Stability

The electrochemical stability window of the separators was evaluated by linear sweep voltammetry (LSV) between 2.8 and 6.0 V at a scan rate of 5 $mV \cdot s^{-1}$. As shown in Figure 11, there were no apparent increase in anodic currents below 4.5 V for all separators, which indicated that PE commercial separator and those electrospinning separators were compatible with the carbonate electrolyte and the PMIA polymer electrolyte prepared in this work was electrochemically stable up to 4.9 V. Furthermore, SiO_2/PMIA separators exhibited slightly higher decomposition voltage, which demonstrated that the modified fibrous separators possessed better electrochemical stability.

Cell Performance

The first five cycle charge-discharge profiles of Li/$LiCoO_2$ cells assembled with pure PMIA membrane and 6 % SiO_2/PMIA membrane as separators and cycled under a voltage range of 2.8-4.2 V at current density of 0.1 C are presented in Figure 12(a) and (b), respectively. It could be known that the first-cycle discharge capacity of the Li/$LiCoO_2$ cell was 137.26 $mAh \cdot g^{-1}$ when pure PMIA membrane served as

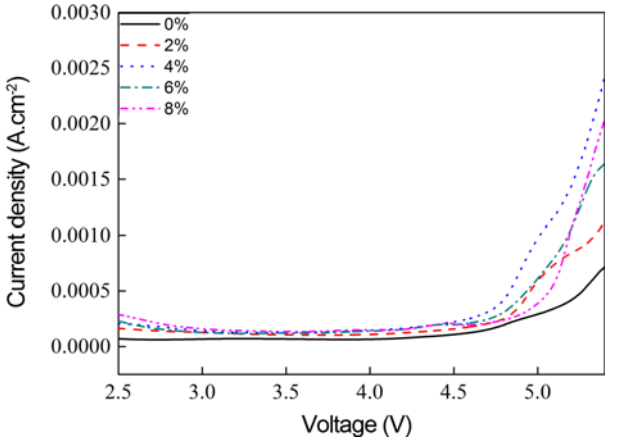

Figure 11. Linear sweep voltammetry of SiO_2/PMIA separators with different SiO_2 contents (0 %, 2 %, 4 %, 6 %, and 8 %) and PE separator.

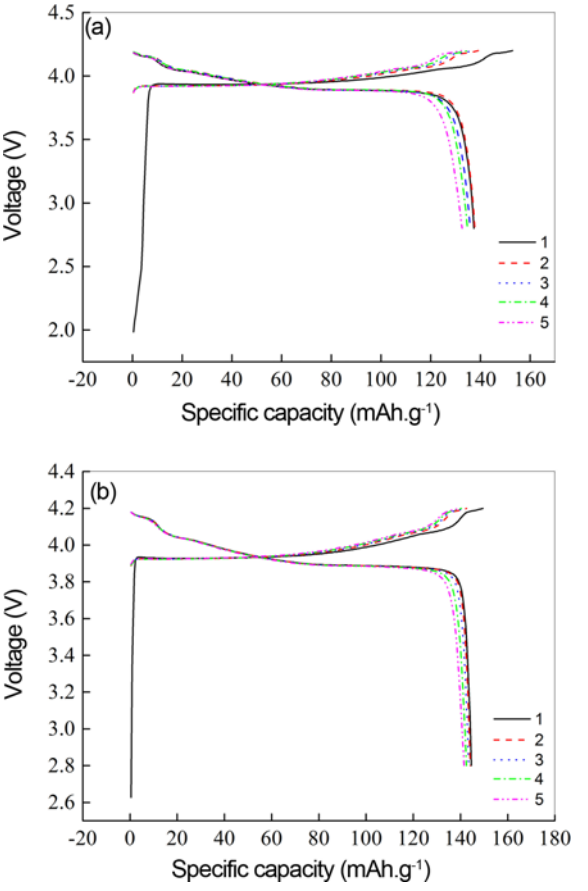

Figure 12. Charge-discharge curves at first 5 times of the cells with pure PMIA membrane (a) and SiO_2/PMIA membrane (6 %, (b)) as separators, cells were cycled at 0.1 C rate between 2.8 and 4.2 V.

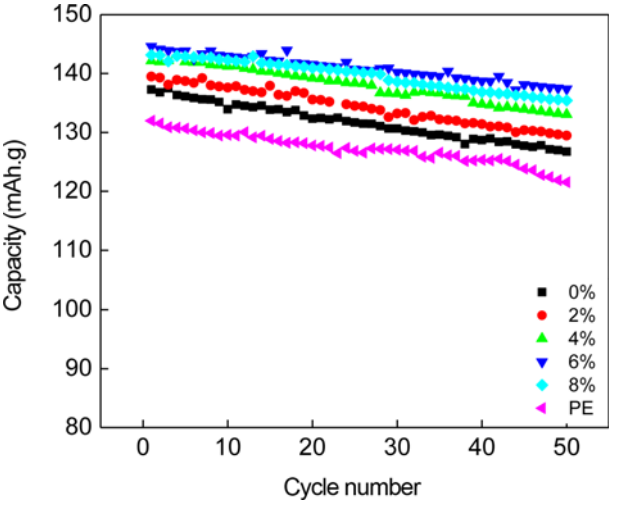

Figure 13. Cycling performance of Li/$LiCoO_2$ cells with SiO_2/PMIA membranes (different SiO_2 content) and PE as separators at 0.1 C.

Table 1. Initial capacity, discharge capacity after 50 cycles and capacity retention of PE and PMIA separators with different SiO_2 contents

Item \ SiO_2 contents	PE	0 %	2 %	4 %	6 %	8 %
Initial capacity ($mAh \cdot g^{-1}$)	131.98	137.26	139.50	142.14	144.61	143.16
Discharge capacity after 50 cycles ($mAh \cdot g^{-1}$)	121.53	126.75	129.46	133.04	137.38	135.43
Capacity retention (%)	92.08	92.34	92.80	93.60	95.00	94.60

bttery separator. The battery with 6 % SiO_2/PMIA membrane attery separator. The battery with 6 % SiO_2/PMIA membrane presented first-cycle discharge capacity of 144.61 $mAh \cdot g^{-1}$. This result indicated that the battery with 6 % SiO_2/PMIA membrane was better in charge-discharge performance than pure PMIA membrane because of the high porosity, electrolyte uptake and ionic conductivity discussed in the sections of ionic conductivities and porosity and electrolyte uptake.

The cycling performance of Li/$LiCoO_2$ cell with PE commercial separator and SiO_2/PMIA separators (different SiO_2 content) is shown in Figure 13. The initial capacity, discharge capacity after 50 cycles and capacity retention of PMIA separators with different SiO_2 contents were presented in Table 1. It could be observed that the cell with the SiO_2/PMIA (6 wt% SiO_2) separator showed higher discharge capacity in all assembled cells. Its discharge capacity after 50 cycles reached to 137.38 $mAh \cdot g^{-1}$ with the capacity retention of 95 %. It was believed that the high porosity and interconnected pores for the electrospinning SiO_2/PMIA separator resulting in high electrolyte uptake and high ionic conductivity, which enhanced the reversibility of lithium ion migration. These results demonstrated that the assembled button batteries showed more excellent cycle performance.

C-rate Performance

Figure 14 shows the C-rate performance of Li/$LiCoO_2$ cell with PE commercial separator and SiO_2/PMIA separators (different SiO_2 content). The cells containing SiO_2/PMIA nanofiber membranes had higher initial discharge capacities than the ones with PE membrane at 0.1 C and they exhibited less capacity fading as the C rate increases. At 5 C, the cells containing PE separator had the lowest discharge capacity of 90.05 $mAh \cdot g^{-1}$ at the 29th cycle. However, the discharge capacity increased to 95.75 $mAh \cdot g^{-1}$ when PMIA nanofiber membrane was used. The discharge capacity further increased to 99.46, 103.76, 104.85 and 103.67 $mAh \cdot g^{-1}$ for cells using 2 %, 4 %, 6 %, 8 % SiO_2/PMIA composite membranes, respectively. It is known that the C-rate performance of the cells is affected by the ionic conductivity and cell resistance [48]. Hence, the outstanding rate capabilities of the cells with SiO_2/PMIA nanofiber membranes could be ascribed to higher ionic conductivities and better interfacial properties of these membranes after up-taking liquid electrolyte. These results confirmed that SiO_2/PMIA composite membranes were promising separator candidates for rechargeable Lithium ion batteries.

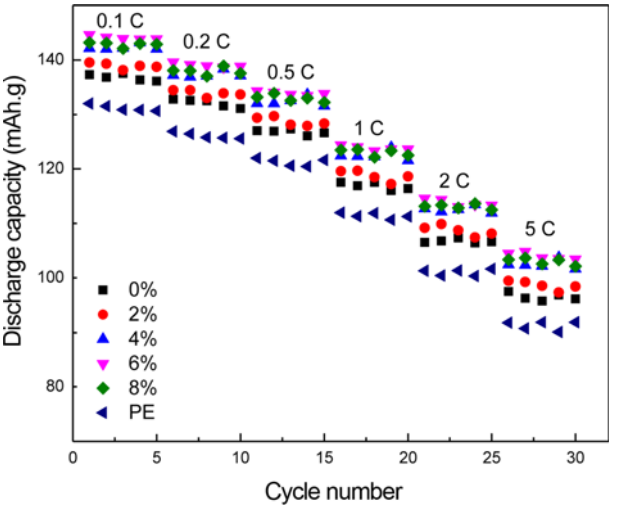

Figure 14. C-rate performance of Li/$LiCoO_2$ cells with SiO_2/PMIA membranes (different SiO_2 contents) and PE as separators.

Conclusion

In summary, SiO_2/PMIA nanofiber membranes were successfully fabricated via the electrospinning technique. The SiO_2/PMIA nanofiber membrane owned robust mechanical properties and excellent thermal stability which was suitable to be an advanced separator for high-performance lithium-ion battery. Benefiting from the three-dimensional network structure, the SiO_2/PMIA composite membrane exhibited high porosity and electrolyte uptake. The addition of 6 wt% SiO_2 enabled the composite membranes demonstrated robust mechanical strength of 18.14 MPa, high ionic conductivity of 3.23×10^{-3} $S \cdot cm^{-1}$ and electrochemical stability up to 4.9 V. Significantly, the Li/$LiCoO_2$ coin cells based on as-prepared PMIA nanofiber membranes with 6 wt% SiO_2 exhibited higher cycling stability compared to PE commercial separator and PMIA nanofiber membranes with other SiO_2 contents based cells. Therefore, the assembled cells with SiO_2/PMIA separators would have a better developmental prospect for the hybrid vehicles in the future.

Acknowledgments

The authors would like to thank National Natural Science Foundation of China (51673148, 51678411), National Key Technology Support Program (2015BAE01B03), Innovation

Fund for Technology of China (14C26211200298), Changjiang Scholars and Innovative Research Team in University of Ministry of Education of China (IRT13084) for their financial support.

References

1. W. Ye, J. Zhu, X. J. Liao, S. H. Jiang, Y. H. Li, H. Fang, and H. Q. Hou, *J. Power Sources*, **299**, 417 (2015).
2. Y. Miao, G. N. Zhu, H. Q. Hou, Y. Y. Xia, and T. X. Liu, *J. Power Sources*, **226**, 82 (2013).
3. X. H. Hou, M. Zhang, J. Y. Wang, S. J. Hu, and X. Liu, *J. Solid State Electr.*, **19**, 3395 (2015).
4. P. Zhao, J. P. Yang, Y. M. Shang, L. Wang, M. Fang, J. L. Wang, and X. M. He, *J. Energy Chem*., **24**, 138 (2015).
5. P. Poizot, S. Laruelle, S. Grugeon, L. Dupont, and J. M. Tarascon, *Nature*, **407**, 496 (2000).
6. M. Raja, G. Sanjeev, T. P. Kumar, and A. M. Stephan, *Ceram. Int.,* **41**, 3045 (2015).
7. S. S. Zhang, *J. Power Sources*, **164**, 351 (2007).
8. M. Yanilmaz, M. Dirican, and X. Zhang, *Electrochim. Acta*, **133**, 501 (2014).
9. Y. Z. Liang, Z. Lin, Y. P. Qiu, and X. W. Zhang, *Electrochim. Acta*, **56**, 6474 (2011).
10. J. Song, M. H. Ryou, B. Son, J. N. Lee, D. J. Lee, Y. M. Lee, J. W. Choi, and J. K. Park, *Electrochim. Acta*, **85**, 524 (2012).
11. H. S. Jeong, S. C. Hong, and S. Y. Lee, *J. Membr. Sci.,* **364**, 177 (2010).
12. M. K. Song, Y. T. Kim, B. W. Cho, B. H. Popov, and H. W. Rhee, *J. Electrochem. Soc*., **150**, A439 (2003).
13. N. Muniyandi, N. Kalaiselvi, P. Periyasamy, R. Thirunakaran, B. R. Babu, S. Gopukumar, N. G. Renganathan, and M. Raghavan, *J. Power Sources*, **96**, 14 (2001).
14. T. Ma, Z. Y. Cui, Q. Ying, H. Shu, H. Wang, F. Yan, N. Han, and J. X. Li, *J. Membr. Sci.*, **444**, 213 (2013).
15. Y. J. Hwang, K. S. Nahm, T. P. Kumar, and A. M. Stephan, *J. Membr. Sci.*, **310**, 349 (2008).
16. Y. H. Ding, P. Zhang, Z. L. Long, Y. Jiang, F. Xu, and W. Di, *J. Membr. Sci.*, **329**, 56 (2009).
17. P. Raghavan, X. H. Zhao, J. Manuel, G. S. Chauhan, J. H. Ann, H. S. Ryu, H. J. Ann, K. W. Kim, and C. Nah, *Electrochim. Acta*, **55**, 1347 (2010).
18. C. Y. Cao, L. Tan, W. W. Liu, J. Q. Ma, and L. Li, *J. Power Sources*, **248**, 224 (2014).
19. Y. Y. Zhai, K. Xiao, J. Y. Yu, and B. Ding, *Electrochim. Acta*, **154**, 219 (2015).
20. X. L. Wu, J. Lin, J. Y. Wang, and H. Guo, *Key Eng. Mat*., **645**, 1201 (2015).
21. D. Z. Wu, C. Shi, S. H. Huang, X. C. Qiu, H. Wang, Z. Zhan, P. Zhang, J. B. Zhao, D. H. Sun, and L. W. Lin, *Electrochim. Acta*, **176**, 727 (2015).
22. H. Lee, M. Alcoutlabi, O. Toprakci, G. J. Xu, J. V. Watson, and X. W. Zhang, *J. Solid State Electr.,* **18**, 2451 (2014).
23. T. Evans, J. H. Lee, V. Bhat, and S. H. Lee, *J. Power Sources*, **292**, 1 (2015).
24. W. L. Li, Y. J. Xing, Y. H. Wu, J. W. Wang, L. Z. Chen, G. Yang, and B. Z. Tang, *Electrochim. Acta*, **151**, 289 (2015).
25. M. Kang, X. M. Ma, H. H. Zhao, J. G. Ju, Y. X. Zhao, J. Yan, and B. W. Cheng, *J. Solid State Electr.*, **20**, 2791 (2016).
26. N. Kimura, T. Sakumoto, Y. Mori, B. S. Kim, K. H. Song, and I. S. Kima, *Compos. Sci. Technol*., **92**, 120 (2014).
27. J. L. Hao, G. T. Lei, Z. H. Li, L. J. Wu, Q. Z. Xiao, and L. Wang, *J. Membr. Sci.,* **428**, 11 (2013).
28. Y. E. Miao, G. N. Zhu, H. Q. Hou, Y. Y. Xia, and T. X. Liu, *J. Power Sources*, **226**, 82 (2013).
29. X. X. Liang, Y. Yang, X. Jin, Z. H. Huang, and F. Y. Kang, *J. Membr. Sci.,* **493**, 1 (2015).
30. Y. Lee, H. Lee, T. Lee, M. H. Ryou, and Y. M. Lee, *J. Power Sources*, **294**, 537 (2015).
31. H. Chen, Q. Lin, Q. Xu, Y. Yang, Z. P. Shao, and Y. Wang, *J. Membr. Sci.,* **458**, 217 (2014).
32. Y. Y. Zhai, N. Wang, X. Mao, Y. Si, J. Y. Yu, S. S. Al-Deyab, M. El-Newehy, and B. Ding, *J. Mater. Chem. A*, **2**, 14511 (2014).
33. Y. J. Wu, J. C. Seferis, and V. Lorentz, *J. Appl. Polym. Sci.,* **86**, 1149 (2002).
34. J. J. Zhang, Q. S. Kong, Z. H. Liu, S. P. Pang, L. P. Yue, J. H. Yao, X. J. Wang, and G. L. Cui, *Solid State Ionics*, **245-246**, 49 (2013).
35. K. Xiao, Y. Y. Zhai, J. Y. Yu, and B. Ding, *RSC Advances*, **5**, 55478 (2015).
36. R. S. Juang, C. T. Hsieh, P. A. Chen, and Y. F. Chen, *J. Power Sources*, **286**, 526 (2015).
37. K. S. Jeon, R. Nirmala, R. Navamathavan, K. J. Kim, S. H. Chae, T. W. Kim, H. Y. Kim, and S. J. Park, *Mater. Lett*., **132**, 384 (2014).
38. M. Yanilmaz, Y. Lu, M. Dirican, K. Fu, and X. W. Zhang, *J. Membr. Sci.,* **456**, 57 (2014).
39. M. Yanilmaz, C. Chen, and X. W. Zhang, *J. Polym. Sci. Pol. Phys*., **51**, 1719 (2013).
40. N. Wu, Q. Cao, X. Y. Wang, S. Li, X. Y. Li, and H. Y. Deng, *J. Power Sources*, **196**, 9751 (2011).
41. J. R. Kim, S. W. Choi, S. M. Jo, W. S. Lee, and B. C. Kim, *J. Electrochem. Soc*., **152**, A295 (2005).
42. W. Xiao, C. Miao, X. M. Yan, and P. Mei, *Polym. Inter*., **65**, 224 (2016).
43. H. F. Zhao, M. Y. Zhang, S. F. Zhang, and J. B. Lu, *Polym. Plast. Technol.*, **51**, 134 (2012).
44. J. Shayapat, O. H. Chung, and J. S. Park, *Electrochim. Acta*, **170**, 110 (2015).
45. W. Jiang, Z. H. Liu, Q. S. Kong, J. H. Yao, C. J. Zhang, P. X. Han, and G. L. Cui, *Solid State Ionics*, **232**, 44 (2013).
46. C. Wang, Y. Wei, G. R. Ferment, W. Li, and T. J. Li, *Mater. Lett.*, **39**, 206 (1999).
47. S. Rajendran and T. Uma, *Mater. Lett.*, **45**, 191 (2000).
48. J. Cao, L. Wang, M. Fang, Y. Shang, L. Deng, J. Yang, J. Li, H. Chen, and X. He, *Electrochim. Acta*, **114**, 527 (2013).